Unraveling the multilayer mechanical response of aorta using layer-specific residual stresses and experimental properties

Clara Díaz [a] Juan A. Peña [b,c] Miguel A. Martínez [a,c,d] Estefanía Peña [a,c,d,*]

[a] *Department of Mechanical Engineering. University of Zaragoza. Spain*

[b] *Department of Management and Manufacturing Engineering. Faculty of Engineering and Architecture. University of Zaragoza. Spain*

[c] *Applied Mechanics and Bioengineering. Aragón Institute of Engineering Research (I3A). University of Zaragoza. Spain*

[d] *CIBER de Bioingeniería, Biomateriales y Nanomedicina (CIBER-BBN). Zaragoza. Spain*

Abstract

To test the capability of the multilayer model, we used previously published layer-specific experimental data relating to the axial pre-stretch, the opening angle, the fiber distribution obtained by polarized light microscopy measurements, and the uniaxial and biaxial response of the porcine descending and abdominal aorta. We fitted the mechanical behavior of each arterial layer using Gasser, Holzapfel and Ogden strain energy function using the dispersion parameter κ as phenomenological parameter obtained during the fitting procedure or computed from the experimental fiber distribution. A multilayer finite element model of the whole aorta with the dimensions of the circumferential and longitudinal strips were then built using layer-specific material parameters previously fitted. This model was used to capture the whole aorta response under uniaxial and biaxial stress states and to reproduce the response of the whole aorta to internal pressure.

Our results show that a model based on a multilayer structure without residual stresses is unable to render the uniaxial and biaxial mechanical response of the aorta ($R^2 = 0.6954$ and $R^2 = 0.8582$ for ddescending thoracic aorta (DTA) and infrarenal abdominal aorta (IAA), respectively). Only an appropriate multilayer model that includes layer-specific residual stresses can reproduce the response of the whole aorta ($R^2 = 0.9787$ and $R^2 = 0.9636$ for DTA and IAA respectively). In addition, a multilayer model without residual stresses produces the same stress distribution as a monolayer model without residual stresses where the maximal value of circumferential and longitudinal stresses appears at the inner radius of the intima. Finally, if layer-specific residual stresses are not available, there is less error the stress distribution using a monolayer model with residual stresses that a multilayer model without residual stresses.

Key words:
Three-layer model, arterial mechanics, residual stresses, aorta

Preprint submitted to J Mech Behav Biomed Mater

1 Introduction

According to the World Health Organization, chronic cardiovascular diseases are the leading cause of death. For this reason, the study of the mechanical factors that induce vascular pathologies is one of the main research lines in Biomechanics. The mechanical variables that strongly influence vascular mechanobiology may be computed thanks to a large number of constitutive relations describing the mechanical response which have been proposed for cardiovascular tissue. (Humphrey, 2002). In this context, the study of the arteries has gained much attention.

Many connective tissues consist of multiple layers composed of proteins such as collagen. One example of a multi-layered tissue structure is the aortic wall. Healthy arteries are composed of three clearly defined layers. The intima (the innermost layer) consists of a single layer of endothelial cells, a thin basal membrane and a subendothelial layer; the media (the middle layer) is composed of a 3D network of elastin, smooth muscle cells and collagen fibres; and the adventitia (the outer layer) consists of fibroblasts, fibrocytes, ground matrix and thick bundles of collagen fibres (Rhodin, 1980). The reason for considering three separate layers also arises from the histology of arteries because the composition and the distribution of the components of the intima, media and adventitia layers (elastin, collagen and cell contents) are different.

Residual stresses in the blood vessel walls are one of the most important features of vascular tissues. Specifically, it is widely accepted in blood vessel modeling that residual stresses play a homogenizing role with regard to the circumferential stress distribution (Chuong and Fung, 1986; Fung, 1993). Since they have a strong influence in the final stress distribution within the arterial wall, it is of paramount importance to include the residual stresses present in a vessel for the accurate modeling of their mechanical behavior under physiological conditions (Alastrué et al., 2007). Residual stresses are defined as those stresses present in the vessels when no loads are applied. It has been shown that the three individual aortic layers, the intima, media and adventitia, undergo drastically different residual deformations upon separation (Holzapfel et al., 2007; Holzapfel and Ogden, 2010; Peña et al., 2015; Sokolis, 2015; Amabili et al., 2019). However, there are few in vitro studies of layer-separated arterial tissue available in the literature (Lu et al., 2003; Holzapfel et al., 2005a; Pandit et al., 2005; Sommer et al., 2010; Sokolis et al., 2012; Weisbecker et al., 2012; Peña et al., 2015; Sassani et al., 2015b,a; Sokolis, 2015; Deveja et al., 2018; Amabili et al., 2019; Sokolis, 2019). Furthermore, residual stresses or mechanical properties are not included in some of these studies. To the best of the authors' knowledge, the studies by Sommer et al. (2010) on human carotid arteries, Peña et al. (2015) on porcine aortas, Sokolis et al. (2012); Sassani et al. (2015b,a) on ascending thoracic aortic aneurysms and Amabili et al. (2019) on human aorta are the only works that present the layer-specific mechanical properties and residual stresses at the same time.

Accurate mechanical models and appropriate numerical approaches can be an asset in the study of cardiovascular dysfunctions and the simulation of surgical interventions, e.g. balloon

* Corresponding author. Tel.: +34876555233; Fax: +34976762578
Email address: fany@unizar.es (Estefanía Peña).

angioplasty or stenting. Computational models require constitutive equations of the vascular tissue. It is possible to develop constitutive models able to accurately reproduce the stress-stretch experimental curves which allow the simulation of the placing of the stent and its interaction with the vessel wall (García et al., 2011). Such models should be based on anatomical information and comprehensive experimental data and help to understand and interpret experimental observations. Therefore, a complete 3-D stress-strain quantification requires separate properties for each of the layers and the inclusion of residual stresses within the constitutive modelling framework. However, quantitative data on residual stresses of each layer are difficult to obtain, so models incorporate residual stresses (RS) without distinguishing the contributions of media and adventitia (Chaudhry et al., 1997; Alastrué et al., 2007; Cilla et al., 2012). In contrast, there are several models in the literature that consider a multilayer model of the aorta neglecting the residual stresses (Holzapfel et al., 2002, 2004; Calvo et al., 2007; Badel et al., 2012; Sáez et al., 2012). Both approaches, using multilayer models without RS or monolayer models with RS, are well established in the literature. However, there is few papers about the influence of both approaches on the stress distribution obtained (Wan et al., 2010; Bellin et al., 2013; Mousavi and Avril, 2017; Maes et al., 2019).

One objective of the paper is to verify the capability of the multilayer model considering layer-specific mechanical properties to capture the whole response of the aorta. To test this capability, we used experimental data taken from a previous work by our group which measured the axial pre-stretch, the opening angle (OA), the fiber distribution, and the uniaxial and biaxial response of the descending thoracic aorta (DTA) and infrarenal abdominal aorta (IAA) (Peña et al., 2015, 2018). We fitted the mechanical behavior of each arterial layer using the uniaxial experimental results. A multilayer model of the whole aorta was then built using layer-specific material parameters. This model was used to capture the whole aorta response under uniaxial and biaxial stress states. Another objective of the paper is to test the hypothesis that the multilayer model with residual stresses (circumferential and axial RS) is the most appropriate model for reproducing the response of the whole aorta. To test this hypothesis, we simulated a multilayer model of idealized descending thoracic aorta using the layer-specific material parameters under diastolic (70 mmHg), physiological systolic (120 mmHg) and supra-physiological systolic (150 mmHg) internal pressure and residual stress. Four models were computed and compared: a three-layer model with residual stresses; a three-layer model without residual stresses; a one-layer model with residual stresses; and a one-layer model without residual stresses.

2 Material and Methods

From all the data from (Peña et al., 2015, 2018), we selected sample II data for our analysis and unpublished data of layer-specific collagen distribution to calibrate the structural model in order to obtain specific constitutive parameters for each layer of the aorta.

2.1 Fitting uniaxial response of layer-specific mechanical properties

To reproduce the mechanical response of each arterial layer, we consider the Gasser, Holzapfel and Ogden (GOH) strain energy function (SEF) (Gasser et al., 2006) that defined the generalized structure tensor $\mathbf{H} = \kappa\mathbf{1} + (1-3\kappa)\mathbf{M}_0$ (where $\mathbf{1}$ is the identity tensor and $\mathbf{M}_0 = \mathbf{m}_0 \otimes \mathbf{m}_0$ is a structure tensor defined using unit vector $\mathbf{m}_0$ specifying the mean orientation of fibers)

$$\Psi = \mu\,(I_1 - 3) + \sum_{i=4,6} \left[\frac{k_1}{2k_2} \left(exp\left\{ k_2 \hat{E}_i \right\} - 1 \right) \right], \tag{1}$$

where $\hat{E}_i = \kappa I_1 + (1-3\kappa) I_i - 1$ for the i-th family of collagen fibres ($i = 4, 6$). In this equation $I_1 = tr\bar{\mathbf{C}}$ represents the first invariant of the modified Cauchy-Green tensor ($\bar{\mathbf{C}} = J^{-2/3}\mathbf{F}^T\mathbf{F}$) characterizing the isotropic mechanical response of the elastin (Gundiah et al., 2009; Lillie et al., 2010) and $\mathbf{F}$ the deformation gradient (Spencer, 1971), while $I_i = \mathbf{m}_{0i} \otimes \mathbf{m}_{0i} : \bar{\mathbf{C}}$ characterize the mechanical response in the preferential directions of the fibers/cells. $\kappa \in [0, 1/3]$ is a dispersion parameter (the same for each collagen fiber family); when $\kappa = 0$, the model is the same as that published in Holzapfel et al. (2000), and when $\kappa = 1/3$ it recovers an isotropic potential similar to that used in Demiray (1972). Note that κ could have histological meaning due to the fully characterized distribution (Gasser et al., 2006), so assuming that the embedded collagen fibres are distributed according to a transversely isotropic and p-periodic Von Mises orientation density function (ODF),

$$\rho(\theta) = 4\sqrt{\frac{b}{2\pi}} \frac{\exp(b[\cos(2\theta) + 1])}{\mathrm{erfi}(\sqrt{2b})}, \tag{2}$$

where the concentration parameter $b \in \mathbb{R}^+$ is a measure of the anisotropy. $b \to 0$ represents an isotropic material, and $b \to \infty$ a transversally isotropic one. Erfi(x) is the imaginary error function. Finally, we can compute κ by the expression (Gasser et al., 2006)

$$\kappa = \frac{1}{4} \int_0^{\pi} \rho \sin^3\theta d\theta. \tag{3}$$

Due to the physiological meaning of κ, we can obtain this parameter by fitting or we can compute the collagen fiber distribution by histological measurements. The present work used polarized light microscopy (PLM) together with a universal rotary stage to identify the three-dimensional structural arrangement of collagen in the aorta (Smith et al., 1981; Canham et al., 1989; Gasser et al., 2012). For this purpose, segments of thoracic and abdominal aorta from Sample II were fixed and prepared for histological analysis. Wall longitudinal specimens, approximately 0.5.0x0.25 cm in size, were prepared from each tissue sample being fixed in formaldehyde for 24 h and then moved to 70% alcohol. Following Gasser et al. (2012), only one slices in the intima, two in the media and one in the adventitia on the tangential plane (circumferential-longitudinal plane) of each specimen, were analyzed. Slides were stained for birefringence enhancement with Picrosirius Red stain (Figure 1), which causes collagen to appear in a brighter orange-yellow color when viewed through polarized light (Canham

et al., 1997, 1989; Smith et al., 1981). The samples were analyzed in a DM2500 M microscope equipped with a DFC295 digital microscope color camera (Leica Microsystems, Germany) and with a Universal Rotary Stage (Carl Zeiss GmbH, Jena, Germany) (Smith et al., 1981). The orientation of a collagen fiber in 3D space was uniquely defined by its elevation angle Φ and its azimuthal angle Θ. However, for modeling purposes we considered only its azimuthal angle Θ for simplicity (Sáez et al., 2016). A least-square minimization procedure with the objective function $\chi^2 = \sum_{i=1}^{n}(\rho_i^{exp} - \rho_i^{ODF})^2$ was used in order to estimate Von Mises ODF ρ_i^{ODF} parameters from the experimentally identified collagen orientation distribution ρ_i^{exp}. A 39th degree discretisation proposed by Heo and Xu (2001) with $n = 600$ integration directions were used.

Accordingly, any continuous integration over the unit sphere can be approximated by a numerical integration

$$\langle(\bullet)\rangle = \frac{1}{4\,\pi}\int_{\mathbb{U}^2}(\bullet)\,\mathrm{d}A \approx \sum_{i=1}^{n} w^i\,(\bullet)_i, \tag{4}$$

where we denote by $\{w^i\}_{i=1,\cdots,n}$ the corresponding weighting factors. Each experimentally measured orientation was assigned to the closest spatial orientation of the corresponding numerical integration direction, p_i being the number of experimental orientations assigned to each integration direction i. In order to fulfill the normalization requirements of the numerical integration, $\frac{1}{4\,\pi}\int_{\mathbb{U}^2}\rho_i^{exp}\,\mathrm{d}A \approx \sum_{i=1}^{n} w^i\,\rho_i^{exp}$, the experimental collagen orientation distribution was defined as $\rho_i^{exp} = \frac{p_i}{\hat{p}}$ where $\hat{p} = \sum_{i=1}^{n}(w^i p_i)$. Finally the quality of the model representation or experimental fitting was assessed by the normalized square error, $NSE = \Sigma_{i=1}^{n}\frac{(\rho_i^{exp}-\rho_i^{ODF})^2}{\rho_i^{exp}}$.

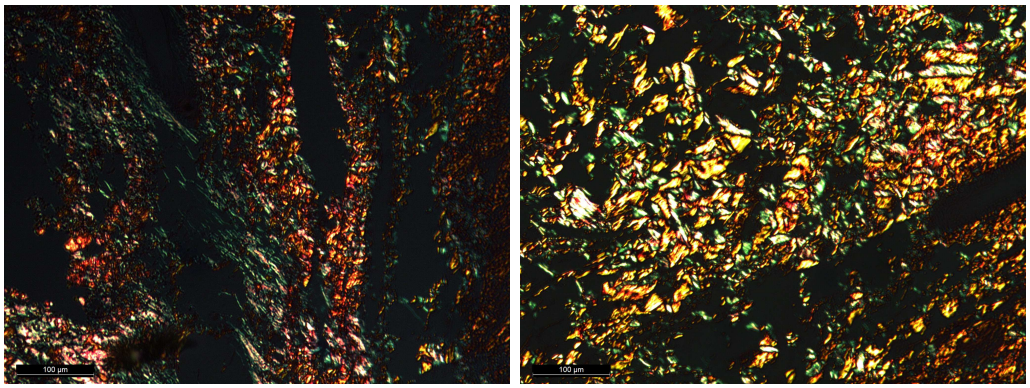

(a) DTA specimen (b) IAA specimen

Fig. 1. Polarized light microscope images taken from the adventitia layer of DTA (left) and the IAA (right) specimens of Sample II.

We fitted the mechanical behavior of each arterial layer at physiological level loads (until 120 kPa) using the uniaxial experimental results of our previous work (Peña et al., 2015) for sample II. The tissue was assumed to be incompressible (Carew et al., 1968), i.e. $\det(\mathbf{F}) = \lambda_1\lambda_2\lambda_3 = 1$, where $\mathbf{F}$ represents the deformation gradient tensor and λ_i, $i = 1, 2, 3$, the stretches in the principal directions. Considering an uniaxial tension test in the longitudinal or circumferential directions, the First Piola-Kirchhoff stress tensor becomes $\boldsymbol{P} = [P_{ii},\ 0,\ 0]$. The fitting of the

experimental data was developed by using a Nelder and Mead type minimization algorithm (Nelder and Mead, 1965) that is a heuristic search method that uses the concept of simplex by defining the objective function Eq.(5). In this function, $P_{\theta\theta}$ and P_{zz} are the First Piola-Kirchhoff (engineering) stress data obtained from the uniaxial tests, $P^{\Psi}_{\theta\theta} = \frac{\partial \Psi}{\partial \lambda_\theta} - p$ and $P^{\Psi}_{zz} = \frac{\partial \Psi}{\partial \lambda_z} - p$ are the analytical First Piola-Kirchhoff stress for the jth point for a homogeneous pure uniaxial state Ψ, where p is a Lagrange multiplier associated with the incompressibility constraint (determined from the equilibrium equations and the boundary conditions) and n is the number of data points.

$$\chi^2 = \Sigma_{j=1}^{n} \left[\left(P_{\theta\theta} - P^{\Psi}_{\theta\theta} \right)_j^2 + \left(P_{zz} - P^{\Psi}_{zz} \right)_j^2 \right]. \tag{5}$$

The traditional coefficient of determination $R^2 \in [0,1]$ and the normalized mean square root error (RMSE) $\varepsilon \in [0,1]$, $\varepsilon = \frac{\sqrt{\frac{\chi^2}{n-q}}}{\varpi}$, were computed for each fitting. In this equation, $\varpi = \frac{\Sigma_{j=1}^{n}(\sigma)_j}{n}$ is the mean value of the measured stresses, q is the number of parameters of the SEF, so $n-q$ is the number of degrees of freedom, and μ the mean stress already defined above. Two different sets of parameters have been considered. First, an optimization procedure of the experimental data considering κ and θ as parameters to be fitted was developed. A total of 5 elastic parameters $(\mu, k_1, k_2, \kappa, \theta)$ had to be fitted (phenomenological set parameters). Another set of parameters was computed considering the κ and θ values obtained from the histological data (structural set parameters). Because κ and θ had been previously computed by histological analysis, a total of only 3 elastic parameters (μ, k_1, k_2) had to be fitted.

In order to prove that the material parameters (phenomenological and structural set parameters) obtained during the fitting procedure can reproduce the behavior of the tissue, a finite element (FE) simulation of the uniaxial experiments was done. The geometric model was reconstructed from the measurements for the whole aorta and the intima, media and adventitia layers for circumferential and longitudinal directions of DTA and IAA for sample II (Peña et al., 2015). A FE model reflecting the boundary conditions of each of the uniaxial tests was created. The specimen arms were held rigidly in clamps and fixed displacements, u_x and u_y were applied. A mesh sensitivity analysis was carried out in order to investigate the model mesh independence. Finally, between 3402 and 6820 eight node brick elements were used depending on the geometry. Force-displacement curves for each computed test were compared with the equivalent experimental data. FE simulations were performed using the Abaqus/Standard v6.13-2 software package.

2.2 Multilayer model of an aorta: validation by uniaxial and biaxial tests

In Peña et al. (2015), the longitudinal and circumferential residual stresses were measured for DTA and IAA specimens. Due to this fact, two different sets of computations were performed using a multilayer model without and with residual stresses, see Tables 1 and 2. In order to include the residual stresses on the aorta using the methodology proposed by Alastrué et al. (2007), and assuming an incompressibility response of the layers, a user subroutine UMAT was implemented in Abaqus. A diagram of the different deformation states appearing during stress

enforcement is represented in Figure 2. The first state Ω_{sf} is defined as the initial stress-free state, corresponding to the initial stress-free geometry. The second state Ω_{lf} is reached by means of a non-compatible tensor $\mathbf{\Psi}_0$ that enforces residual stresses in the solid. Since $\mathbf{\Psi}_0$ may lead to an unbalanced situation, a third compatible state appears. $\mathbf{F}_{comp}$ maps the Ω_{lf} configuration into Ω'_{lf} enforcing the equilibrium conditions. These two configurations should be very similar if the non-compatible tensor $\mathbf{\Psi}_0$ is properly chosen. In other words, $\mathbf{F}_{comp}$ should be very close to $\mathbf{I}$, which means that the deformations between Ω_{lf} and Ω'_{lf} should be very close to zero and the stresses in states Ω_{lf} and Ω'_{lf} should be almost the same. The fourth configuration Ω_l is the result of applying the external load onto the model with the deformation gradient tensor $\mathbf{F}_{load}$. Therefore, the whole deformation gradient between the stress free configuration Ω_{sf} and the physiological state Ω_l is defined as $\mathbf{F}_t = \mathbf{F}_{load}\mathbf{F}_{comp}\mathbf{\Psi}_0$. To introduce residual stresses into the finite element formulation, it is necessary to specify $\mathbf{\Psi}_0$ pointwise within the finite element mesh. An equilibrium step is then applied with zero forces obtaining $\mathbf{F}_{comp}$. A second load step will result in the deformation gradient $\mathbf{F}_{load}$ that balances the externally applied forces.

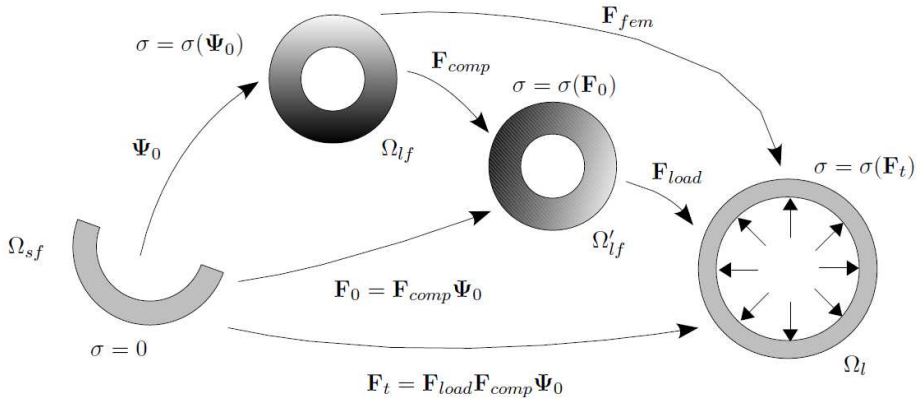

Fig. 2. Deformation gradient decomposition diagram.

A multilayer model of DTA and IAA samples was built using the whole sample dimensions and the thickness ratio between intima-media-adventitia (0.21:0.48:0.31 and 0.30:0.54:0.16 for DTA and IAA, respectively) obtained for sample II (Peña et al., 2015), see Figure 3.a and Tables 1 and 2. The previously fitted layer-specific material parameters (phenomenological and structural set parameters) for the intima, media and adventitia were used to reproduce the uniaxial response of the whole aorta, i.e. the set of parameters $(\mu, k_1, k_2, \kappa, \theta)$ that were identified by the fitting procedure for the layer samples, were used to capture the mechanical data of the whole aorta. The joints between the intima-media and the media-adventitia were modelled as a perfectly bonded interface. As described in the previous section, the specimen arms were held rigidly in clamps and fixed displacements, u_x and u_y were applied. Between 8514 and 11770 hexahedral elements were used depending on the geometry. Again, force-displacement curves for the FE models with and without residual stresses were computed and compared with the experimental data for whole DTA and IAA specimens and each direction of sample II as presented in Peña et al. (2015).

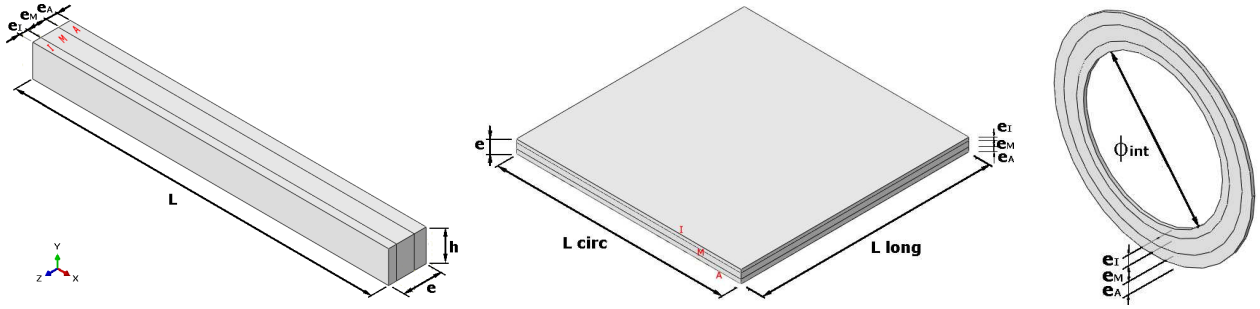

(a) Uniaxial (b) Biaxial (c) Inflation

Fig. 3. Geometry for the multilayer model of uniaxial, biaxial and cylindrical inflation cases for the aorta. Uniaxial, biaxial and inflation samples were built using the whole sample with dimensions and thickness ratio between intima-media-adventitia of 0.21:0.48:0.31 and 0.30:0.54:0.16, respectively. e: thickness, h: weight, L: length and ϕ_{int}: diameter.

Longitudinal residual stresses were computed directly by measuring λ_z^{res} from the experiments developed by Peña et al. (2015) while the curling of axial strips was disregarded. Regarding the circumferential stresses, on the whole aorta part of the arterial specimen undergoes tension, while the opposite side experiences compression. After the OA experiment, the main part of the stress distribution is released and the remaining stresses are due to the fact that each layer has different OAs. We compute the remaining circumferential residual stresses of each layer by using the geometry data of the opened sector of the whole sample and of each layer, and approximate by a uniform value corresponding to the mean of the $\lambda_\theta(r)$ of the inner and outer walls λ_{θ_i} and λ_{θ_0} respectively. So, the stresses associated with radially-cutting rings have been disregarded.

	DTA				IAA			
	Intima	Media	Adventitia	Whole	Intima	Media	Adventitia	Whole
Thickness [mm]	0.500	1.100	0.740	2.830	0.477	0.817	0.240	1.517
Length [mm]	28.380	28.540	31.770	26.800	27.850	25.380	30.060	24.940
Width [mm]	2.790	2.500	2.880	2.390	2.190	2.310	2.240	2.630
λ_{theta}^{res} [-]	0.9541	1.0334	0.9286	-	1.0154	1.0162	0.9593	-

Table 1
Geometry and in situ stretch of intima, media, adventitia and whole aorta from (Peña et al., 2015) for DTA and IAA circumferential specimens of Sample II

Regarding the biaxial response of the aorta, a multilayer model with and without residual stresses of square specimens of 35 x 35 mm were created for the DTA, see Tables 1 and 2, and Figure 3.b. Only experimental data for the DTA specimen is available, so we can only validate the model for this sample. Again, we consider the thickness ratio between the intima-media-adventitia of uniaxial specimens. The layer-specific material parameters (phenomenological and structural) fitted as described in the previous section were also included. A mesh with approximate 7500 eight node brick elements were selected. The biaxial boundary conditions

	DTA				IAA			
	Intima	Media	Adventitia	Whole	Intima	Media	Adventitia	Whole
Thickness [mm]	0.520	0.930	0.717	2.800	0.420	0.610	0.217	1.453
Length [mm]	21.950	24.640	22.570	20.620	13.830	18.400	14.674	21.580
Width [mm]	2.203	2.363	2.660	3.560	2.247	2.320	2.290	2.640
λ_z^{res} [-]	0.9570	1.0384	0.9521	-	0.9645	1.0053	0.9427	-

Table 2
Geometry and in situ stretch of intima, media, adventitia and whole aorta from (Peña et al., 2015) for DTA and IAA longitudinal specimens of Sample II

were prescribed, which left the specimen's edges free to expand laterally and longitudinal and circumferential loads were applied at the edge of the sample. The biaxial response of the multilayer model with and without residual stresses was compared with the experimental results for sample II presented in Peña et al. (2015).

2.3 Three-layer model of an idealized aorta

After validation of the DTA material parameters using the biaxial results, a multilayer model of an idealized cylindrical DTA aorta was built using the whole sample dimensions and the previously obtained thickness ratio between the intima-media-adventitia, see Figure 3.c. The dimensions of the cylinder, i.e., the inner radius and thickness correspond to the sample II reported in Peña et al. (2015) were considered, see Table 3. As commented above, the choice of $\mathbf{\Psi}_0$ is arbitrary and should be specified pointwise. Nevertheless, a proper choice of tensor should result in a $\mathbf{F}_{comp}$ tensor very close to $\mathbf{I}$ (ideally, $\mathbf{F}_{comp} = \mathbf{I}$). Among all the possibilities for determining the residual strains field, we chose the one proposed by Chuong and Fung (1986). We then assumed that the opening angle problem can be modeled as a pure bending problem. The aorta was considered as a thick-walled cylindrical tube. Assuming incompressibility, the residual deformation gradient tensor $\mathbf{F}_{o_i}$ of each i layer can be written as a function of the principal stretches and the unitary vectors of the bases defined in the opened and in the closed configurations of the idealized cylinder, see Alastrué et al. (2007).

$$\mathbf{F}_{o_i} = (\lambda_\theta \lambda_{z_i}^{tot})^{-1} \mathbf{e}_r \otimes \mathbf{E}_R + \lambda_{\theta_i} \mathbf{e}_\theta \otimes \mathbf{E}_\Theta + \lambda_{z_i}^{tot} \mathbf{e}_z \otimes \mathbf{E}_Z \tag{6}$$

where λ_z and $\lambda_\theta(R) = \frac{\kappa r}{R}$ are the in situ stretch, $\kappa = \frac{2\pi}{(2\pi - \alpha)}$ is a measure of the OA α, $\{\mathbf{E}_R, \mathbf{E}_\Theta, \mathbf{E}_Z\}$ is the cylindrical coordinate system in the opened configuration and $\{\mathbf{e}_r, \mathbf{e}_\theta, \mathbf{e}_z\}$ is the cylindrical coordinate system in the closed configuration. For more details see (Alastrué et al., 2007).

The measured OA (α) were 127º, 67º, 73º and 76º for the intima, media, adventitia and whole aorta of the DTA specimen from Sample II (Peña et al., 2015). Finally, the total longitudinal in situ stretch of each i layer (λ_{z_i}) was computed as the composition of the measured $\lambda_{z_i}^{res}$ of each layer and the $\lambda_{z_{whole}}^{res}$, i.e., $\lambda_{z_i}^{tot} = \lambda_{z_{whole}}^{res} \lambda_{z_i}^{res}$, see Table 3.

DTA					
	α [º]	R_i [mm]	r_i [mm]	h [mm]	λ_z^{res} [-]
Intima	127	17.51	5.04	0.324	0.957
Media	67	9.96	5.53	1.389	1.038
Adventitia	73	10.035	6.42	0.545	0.9521
Whole	76	10.09	4.99	2.090	1.198

Table 3
Geometrical parameters needed to estimate the in situ stretch of the intima, media, adventitia and whole aorta from Peña et al. (2015) for DTA specimens from Sample II. R_i and r_i represent the internal radius of the aorta in the opened and closed configurations, respectively, and h is the thickness of the ring in the opened configuration.

The layer-specific material parameters (phenomenological and structural set parameters) for the intima, media and adventitia were used to reproduce the mechanical data of the whole aorta for DTA specimens from Sample II. The joint between intima-media and media-adventitia were modeled again as a perfectly bonded interface. The cylinder was meshed with 675 hexahedral eight node elements per axial layer with only two elements were taken into account in the axial direction, and plane strain boundary conditions were applied. The effect of the layer-specific residual stresses under internal physiological and supra-physiological pressures were studied. Diastolic 9.33 kPa (70 mmHg), physiological systolic 16 kPa (120 mmHg) and supra-physiological systolic 20 kPa (150 mmHg) pressures were considered.

3 Results

3.1 Fitting uniaxial response of layer-specific mechanical properties

Von Mises ODF ρ_i^{ODF} was fitted from the experimentally identified collagen orientation distribution ρ_i^{exp}a. κ parameter is computed from the Von Mises ODF ρ_i^{ODF} parameter b by Equation (3). Figure 4 illustrates that collagen in the porcine aorta predominantly aligns into two families of fibers. Higher dispersion of the collagen fibers were found in the intima and adventitia layers and a more concentrated distribution was found in the media layer, aligned with the circumferential direction. In addition, almost all the samples exhibit two distinct families of collagen fibers with respect to their azimuthal angle.

The uniaxial experimental data reported in our previous work (Peña et al., 2015) for sample II were fitted using the proposed SEF following the procedure explained in Section 2.1. The results considering κ and θ as fitting parameters (phenomenological set parameters) and considering the κ and θ values obtained from the histological data (structural set parameters) are shown in Table 4. Our results indicated that the best fitting was in general with the GOH SEF using the phenomenological parameters, especially for the IAA media sample, showing a RMSE

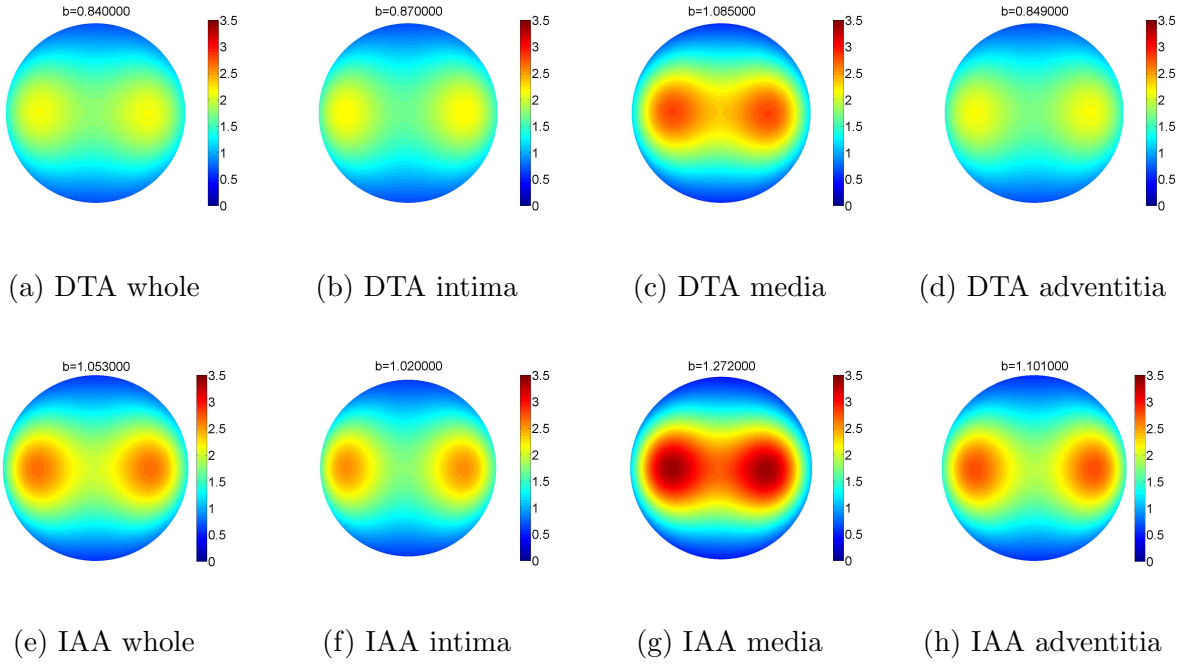

(a) DTA whole (b) DTA intima (c) DTA media (d) DTA adventitia

(e) IAA whole (f) IAA intima (g) IAA media (h) IAA adventitia

Fig. 4. Color-coded and stereographic mapping of the Von Mises orientation distribution function (ODF) where b is the concentration parameter. The data represent the collagen fiber orientations in the DTA (top) and IAA (bottom) wall of the porcine aorta sample II

of $\varepsilon = 0.0263$. In all cases, we obtained the worst fitting using the microstructural GOH parameters. This is because the phenomenological GOH SEF has more parameters than the microstructural, so it is able to identify an appropriate set of parameters that reduce the error between experiments and analytical predictions. For both sets of parameters and the DTA and IAA positions, the worst fitting was for the adventitia layer showing a RMSE of $\varepsilon = 0.0263$ and $\varepsilon = 0.2513$ for the phenomenological and microstructural set of parameters for DTA and $\varepsilon = 0.2518$ and $\varepsilon = 0.1742$ for IAA, respectively. When the distribution of the fibers is included in the fitting procedure, we obtain lower dispersion parameters (κ) and higher orientation angles (θ close to 45°) than the real measured data for the whole aorta and the intima and media layers. These fitting parameters are close to the experimental ones for the adventitia layer, however this fitting is not accurate for DTA. Optimization is a difficult task, especially when the many parameters of the hyperelastic constitutive equation are the terms to be optimized. The solution is not unique and the fitted parameters have no physical meaning.

For the validation of the mechanical constitutive model parameters, uniaxial tests for the descending thoracic aorta and infrarenal abdominal aorta curves of each layer were simulated by FE models separately. Figure 5 shows overlays of the experimental and model-predicted measured load [mN] versus extension [mm] on the grips of the uniaxial test. As can be seen from the plots the correlation of the model responses is satisfactory. Similar to the results of the fitting process, the best correlation between the experimental and FE predicted load was in general with the GOH SEF using phenomenological parameters.

DTA	Phenomenological parameters						Microstructural parameters						
Specimen	μ	k_1	k_2	κ	θ	ε	μ	k_1	k_2	b	κ	θ	ε
Whole	11.86	77.69	20.38	0.150	42.95	0.080	13.66	161.01	24.35	0.840	0.248	39.92	0.133
Intima	22.68	55.73	28.57	0.042	44.72	0.057	22.57	276.45	42.85	0.870	0.246	42.85	0.135
Media	24.74	184.31	30.19	0.261	27.19	0.030	14.30	290.22	4.87	1.085	0.224	35.01	0.106
Adventitia	13.79	139.21	315.28	0.330	16.56	0.238	1.61	278.86	87.62	0.849	0.275	42.78	0.251
IAA													
Whole	7.80	68.56	6.59	0.015	42.24	0.086	7.31	246.70	8.03	1.053	0.225	39.29	0.102
Intima	16.80	75.31	12.42	0.002	43.36	0.070	15.88	297.73	22.45	1.020	0.228	42.51	0.126
Media	13.33	73.84	8.25	0.016	39.40	0.026	17.57	170.85	19.93	1.272	0.204	34.03	0.035
Adventitia	47.37	118.93	124.93	0.251	27.99	0.047	28.26	450.42	0.010	1.101	0.231	38.21	0.174

Table 4
Material constants obtained for the descending thoracic aorta (DTA) and infrarenal abdominal aorta (IAA) curves. For microstructural parameters, κ and θ values were obtained from the histological data. Constants μ and k_1 in MPa, θ in degrees, k_2, κ and b are dimensionless.

3.2 Uniaxial and biaxial response of the whole aorta

To illustrate the multilayer response related to the experimental mechanical properties of the whole samples, plots of the averaged stress-stretch response together with the underlying experimental data are depicted in Figure 6 for the phenomenological and microstructural parameters. Figure 6 compares the results for the multilayer model considering and neglecting residual stresses. The average Cauchy stresses were determined as $\sigma_{\theta\theta} = \frac{F_\theta}{t_\theta w_\theta}\lambda_\theta$ and $\sigma_{zz} = \frac{F_z}{t_z w_z}\lambda_z$, where $t_{\theta,z}$ and $w_{\theta,z}$ are the initial thickness and width respectively. $F_{\theta,z}$ are the sum of the reaction loads on the node clamps of the FE model and $\lambda_{\theta,z}$ are the stretch computed as $\lambda_{\theta,z} = 1 + \frac{u_{\theta,z}}{L_{\theta,z}}$. Finally, $u_{\theta,z}$ are the displacements of the node clamps of the FE model and $L_{\theta,z}$ the distance between clamps for circumferential and longitudinal samples.

It is observed in Figure 6 that both sets of parameters provide a good approximation of the experimental data if the residual stresses are included. Regarding the uniaxial response when residual stresses are included, we obtained a better fitting for the DTA sample using the microstructural set of parameters ($R^2 = 0.9787$) than the phenomenological parameters ($R^2 = 0.8783$) for the circumferential direction and a worse fitting for the longitudinal direction. For the IAA sample, we obtained better fittings in both directions using the phenomenological ($R^2 = 0.9636$) rather than the microstructural parameters ($R^2 = 0.8557$). This could be explained by observing Figure 5 which shows that the worst fittings of the separated layers were obtained for the microstructural set of parameters. Nevertheless, substantial differences between the multilayer models and the experimental results can be observed, when residual stresses are neglected. We obtained a better fitting for the DTA sample using the microstructural set of parameters ($R^2 = 0.8316$) than the phenomenological parameters ($R^2 = 0.6954$). For the IAA sample, we also obtained better fittings using the microstructural ($R^2 = 0.8846$) rather than the phenomenological parameters ($R^2 = 0.8582$). The stress-stretch curves provided by both sets of parameters along the circumferential and longitudinal directions are stiffer than the experimental ones. Nevertheless, more pronounced differences are found in

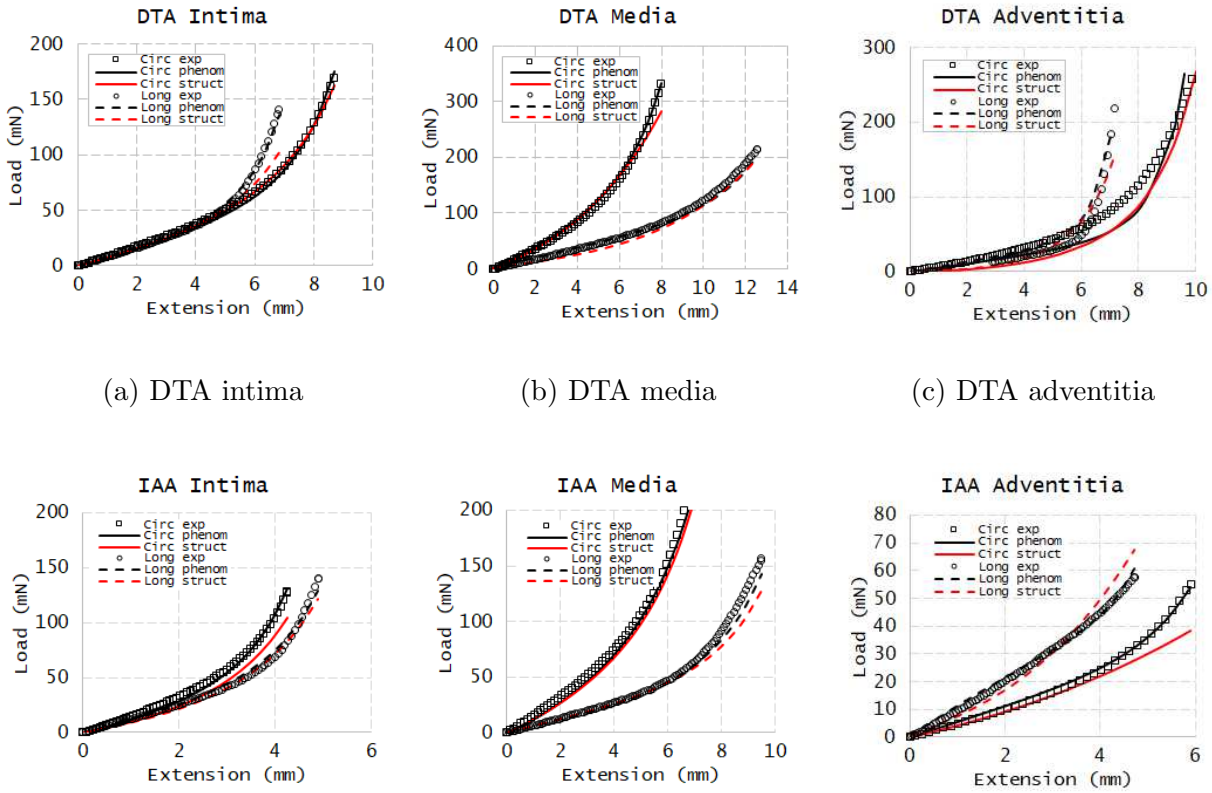

(a) DTA intima (b) DTA media (c) DTA adventitia

(d) IAA intima (e) IAA media (f) IAA adventitia

Fig. 5. Experimental uniaxial tensile tests (Load versus extension) of DTA and IAA samples compared to FE predictions based on SEF of Eq. (1) and the material properties of Table 4. The black line corresponds to the numerical FE approximation using the phenomenological set parameters and the gray line corresponds to the numerical FE approximation using the structural set parameters. Exp: experimental data, phenom: fitting with phenomenological set parameters and struct: fitting structural set parameters

the circumferential direction. For example, a stress value of about 170 kPa was obtained for a stretch of 1.35 for the DTA circumferential experiments, Figure 6.a, whereas the corresponding value provided by the model using the phenomenological set of parameters is far out of the scale of the graph shown.

Contour plots of the Cauchy stress distribution of FE based on multilayer models with and without residual stresses and the phenomenological properties of Table 4 are presented in Figure 7. There are two main findings from this Figure . (i) We notice the discontinuity caused by the inhomogeneous composition of the multilayer model. The combined effect of prestress and the load exerted by the clamps reduced the stress discontinuity between layers. With the exception of the circumferential DTA sample, we obtain a quasi-uniform stress distribution along the sample thickness. Although the intima has compression residual stresses, the highest stress is located at the innermost radius on the intima due to the elevated stiffness response of the layer, as we can see in Figures 5.a and b. We found a similar response for the adventitia. For

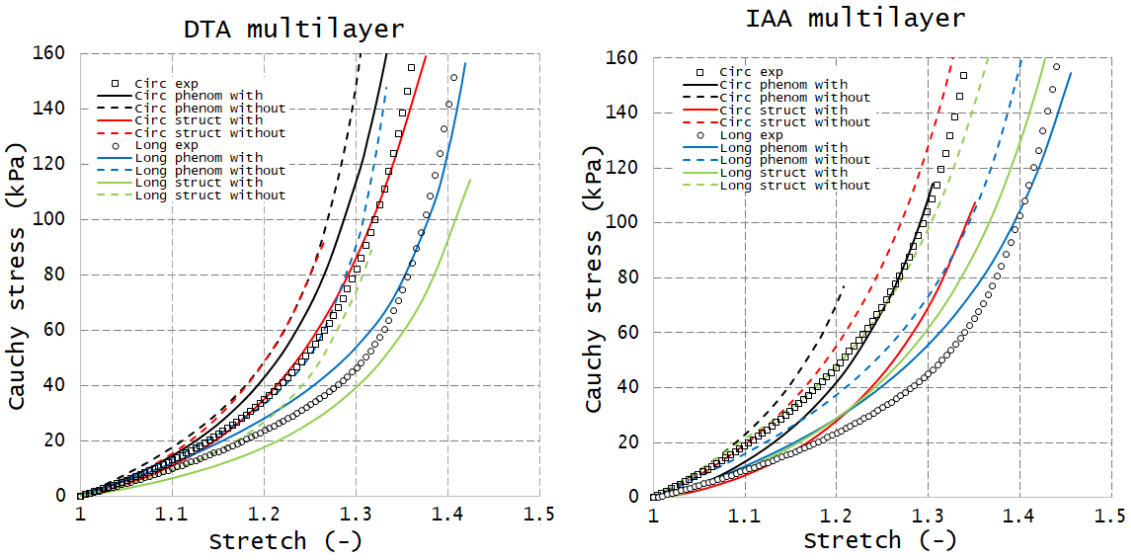

(a) DTA (b) IAA

Fig. 6. Experimental uniaxial tensile tests (stress versus stretch) of DTA and IAA whole samples compared to FE predictions based on multilayer model with and without residual stresses and and the material properties of Table 4 for the corresponding layer. Exp: experimental data, phenom: fitting with phenomenological set parameters and struct: fitting structural set parameters

the models without residual stresses, the stress jump was much more important. Specifically, in the IAA and longitudinal DTA samples, stress at the intima and adventitia layers were higher than that at the media layer, but the opposite was observed for the circumferential DTA sample. (ii) Non physiological stresses were obtained when residual stresses were neglected. For example, stresses between 200 to 350 kPa were observed for the intima and adventitia layers without residual stresses, while the stress on models with prestress were between 95 and 140 kPa. Taking the effects of residual stresses into account did not substantially alter the stresses at the media layer. These non physiological stresses explain the divergence results of the stress versus stretch curves plotted in Figure 6 between the multilayer models without residual stresses and the experimental data. Similar results were obtained for the set of microstructural parameters (data not shown).

Finally, the results for the biaxial test of the DTA whole sample II compared to FE predictions based on a multilayer model with and without residual stresses and the material properties of Table 4 for the each layer are shown in Figure 8. The average Cauchy stresses were determined as $\sigma_{\theta\theta} = \frac{F_\theta}{t_z w_z}\lambda_\theta$ and $\sigma_{zz} = \frac{F_z}{t_\theta w_\theta}\lambda_z$, where $t_{\theta,z}$. $F_{\theta,z}$ are the sum of the reaction loads on the node clamps of the FE model and $\lambda_{\theta,z}$ are the stretch computed as $\lambda_{\theta,z} = 1 + \frac{u_{\theta,z}}{L_{\theta,z}}$. Finally, $u_{\theta,z}$ are the displacements of the node clamps of the FE model and $L_{\theta,z}$ the distance between the clamps for the circumferential and longitudinal samples. The predictive capacity of the multilayer models fitted using uniaxial tests to reproduce the biaxial response of the tissue are better for the models which consider residual stress providing a reasonable approximation of the experimental data of the equibiaxial test (2:2) and the biaxial tests (2:1 and 1:2). The

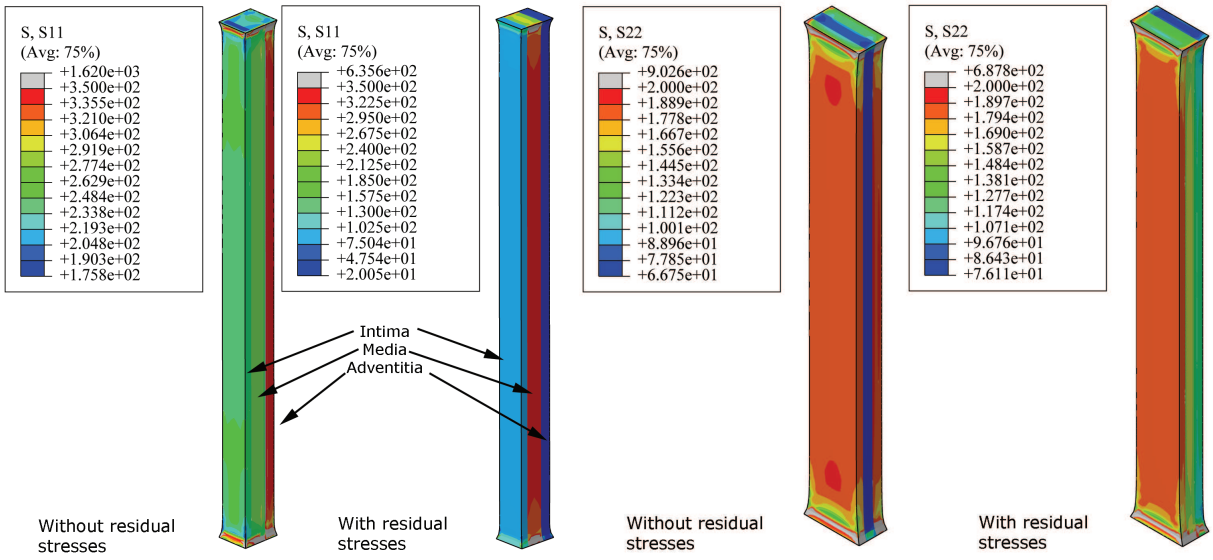

(a) DTA circumferential

(b) DTA longitudinal

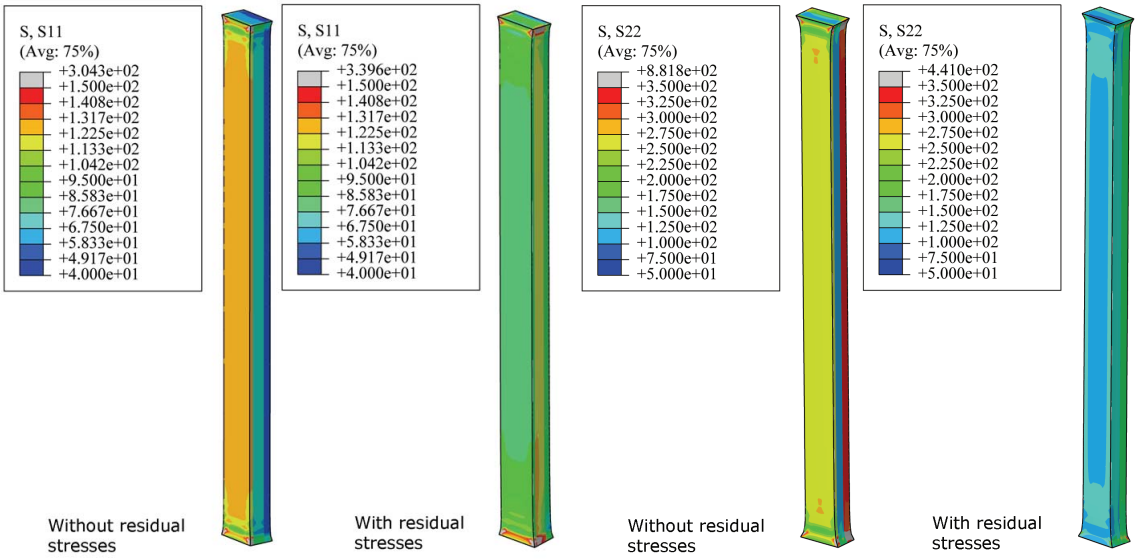

(c) IAA circumferential

(d) IAA longitudinal

Fig. 7. Cauchy stress contour plot [kPa] of uniaxial FE multilayer models with and without residual stresses and the material properties of Table 4 for (a,b) DTA and (c,d) IAA samples. Intima, media and adventitia are indicated by the arrows in (a) and the same locations were replicated in the other cases.

multilayer model without residual stresses was not able to capture the passive biaxial properties of the whole aorta over a wide range of biaxial deformations. The microstructural parameters were able to better reproduce the biaxial deformations showing better predictive capacity in spite of the worse fitting properties on the uniaxial tests.

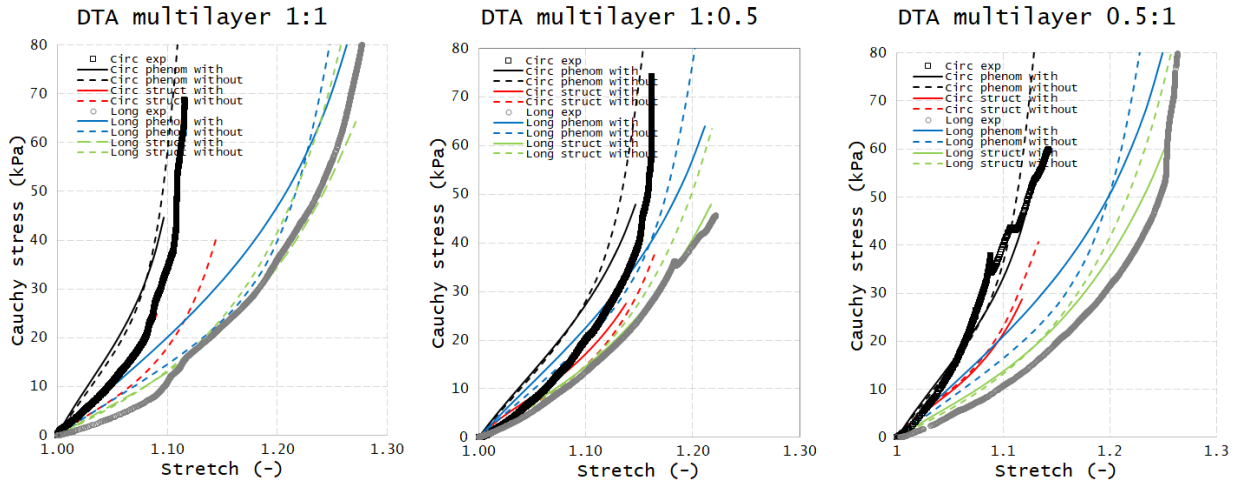

(a) 1:1 (b) 1:0.5 (c) 0.5:1

Fig. 8. Experimental biaxial tensile tests (stress versus stretch) of DTA whole sample II compared to FE predictions based on multilayer models with and without residual stresses and the material properties of Table 4 for the each layer.

Regarding stress maps, Figure 9 shows the predicted mechanical response of the biaxial samples at $\lambda = 1.10$ for the FE multilayer model with and without residual stresses. Similar results to the uniaxial case have been obtained. Figure 9.a demonstrates the relatively high values of the circumferential stress in the media compared with that in the adventitia with residual stresses. Nevertheless, when the residual stresses are neglected, the high values of the circumferential stress are located in the adventitia with non-physiological values. It is noticeable that there is a significant discontinuity in the circumferential stress across the thickness, and a smaller discontinuity in the longitudinal stress. Whereas there is no essential difference in the thickness behavior in the longitudinal direction between the models with and without residual stresses, the global behavior has some significant differences, as shown in Figure 8.

3.3 Three-layer model of an idealized aorta

Four different sets of results are compared in this section corresponding to four FE models: three-layer and one-layer models with circumferential and longitudinal residual stresses and three-layer and one-layer models without residual stresses.

The inhomogeneous nature of the three-layer model affects the circumferential residual stress distribution. In the intima, compressive stress is presented in the innermost radius; its minimal value was about -5.19 kPa. We observed that the stress value increased until reaching its maximal value of 2.44 kPa at the interface between the intima and media. At the innermost radius of the media, the circumferential stress was again compressive with a minimum value of -15.39 kPa . This value was much lower than that in the intima. Therefore, a stress jump of 17.83

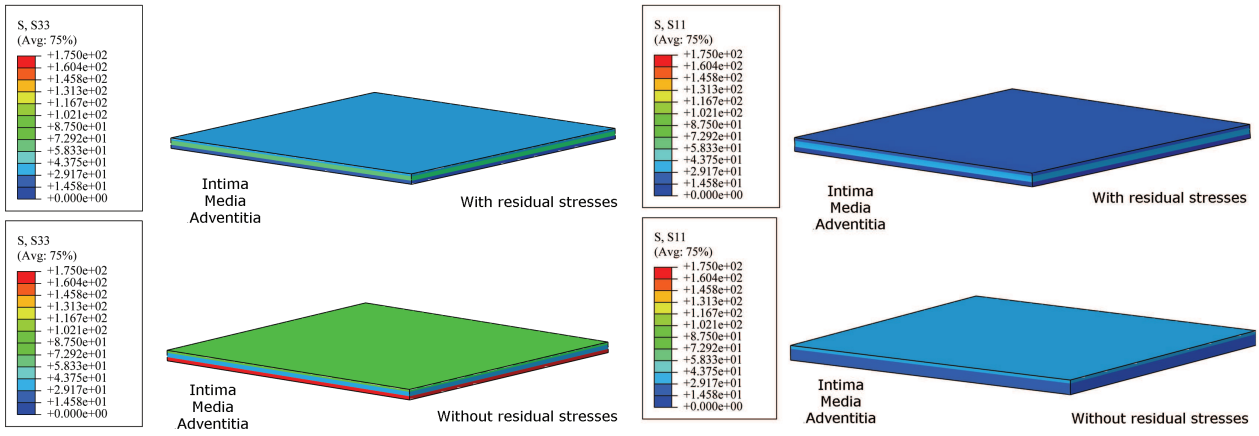

(a) DTA circumferential (b) DTA longitudinal

Fig. 9. Cauchy stress contour plot [kPa] of biaxial FE multilayer models with and without residual stresses at $\lambda = 1.10$. (a) circumferential stress map and (b) longitudinal stress map. Intima, media and adventitia are located on the top, middle and bottom of the sample, respectively.

kPa appeared. We found compressive stress through its whole thickness with the maximum value of -7.74 kPa at the interface between the media and adventitia. We found tension in the adventitia through its whole thickness. At the innermost radius of the adventitia, the circumferential stress had a value of 7.54 kPa. This value was much higher than that in the media. Therefore, a stress jump of 15.28 kPa appeared. From this minimal stress value in the inner radius, the stress increased to the outer radius of the adventitia, where a value of 15.18 kPa was computed. However, the well-known residual stress distribution was obtained when $\mathbf{F}_{o_i}$ from Eq (6)) was applied to the one layer model, Figure 10b. A compressive stress of -10.9 kPa was found in the inner radius with increasing relative value when moving to the outermost radius, where a tensile stress of 8.71 kPa appears.

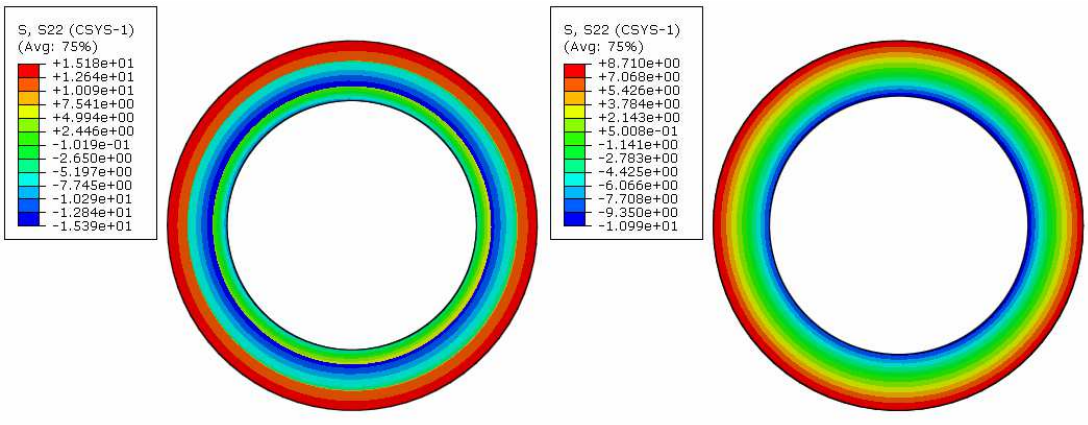

Fig. 10. Circumferential residual stress distribution [kPa] when $\mathbf{F}_{o_i}$ from Eq (6) with data from Table 3 was applied. (a) three layer model and (b) one layer model.

Results for internal diastolic (70 mmHg), physiological systolic (120 mmHg) and supra-physiological systolic (150 mmHg) pressure application are shown in Figure 11. Now, the whole thickness of the cylinder is in tension. It can be clearly observed how the inclusion of residual stresses in the model strongly modifies circumferential stress maps. Maximal circumferential stress values appear in the inner radius when no residual stresses are considered whereas they appear in the outermost radius when residual stresses are accounted for. This effect is more evident for the multilayer model where the stress distribution is more uniform. We again notice the discontinuity caused by the inhomogeneous composition of the three layers. The minimal circumferential stress appeared at the media (37, 46 and 54 kPa at 70, 120 and 150 mmHg respectively) and the maximal at the adventitia (75, 110 and 140 kPa at 70, 120 and 150 mmHg respectively). As in the case of the residual stress map, we can clearly distinguish the interface between the intima-media and media-adventitia, finding that the adventitia bears most of the load at supra-physiological systolic pressure. A well-known circumferential stress map was obtained using the monolayer model under internal pressure and residual stresses. The minimum stress always appeared in the intima, at the inner radius, reaching a value of 44, 52 and 86 kPa at 70, 120 and 150 mmHg respectively. Again the maximum stress was located at the outer radius of the adventitia with values of 61, 80 and 94 kPa at 70, 120 and 150 mmHg respectively. We observe a more homogeneous circumferential stress distribution for the monolayer model than for the three layer model with a lower stress gradient (8 kPa) at supra-physiological systolic (150 mmHg) pressure.

When only the internal pressure is applied, the stress distribution is the well-known distribution for a cylinder under internal pressure. Maximal circumferential stress values appear in the inner radius when no residual stresses are considered, reaching values of 104, 173 and 249 kPa at 70, 120 and 150 mmHg, respectively, for the three layer model and 96, 162 and 227 kPa at 70, 120 and 150 mmHg, respectively, for the one layer model. Unlike the case of the prestressed aorta, we can not clearly distinguish the interface between the intima-media and media-adventitia at systolic pressures (120 and 150 mmHg) for the multilayer model.

In Figure 12, we can appreciate the effect on the circumferential, longitudinal and radial stresses caused by residual stresses with the monolayer and three-layer models . The curve marked "with- out RS" represents the stress distribution without residual stress. We observe the maximal value of circumferential and longitudinal stresses at the inner radius of the intima and a de- creasing gradient to the adventitia, where the stresses decreased to quite low values. In contrast, a positive gradient of the radial stress is obtained which is lower than the stress gradient of the circumferential and longitudinal stresses. We clearly observe the discontinuity caused by the non-homogeneous composition of the aorta for the multilayer model. The stress distribution obtained using the monolayer model shows similar tendency than the discontinuous results obtained with the multilayer model.

The effect of the pressure level on the stress is also observed in Figure 12. Differences in the stress distribution between the multilayer and monolayer models increase when the pressure level increases. The discontinuity caused by the non-homogeneous composition of the aorta is maximal for supra-physiological systolic and minimal for physiological diastolic pressures. These differences are more marked for the circumferential and longitudinal stress distribution

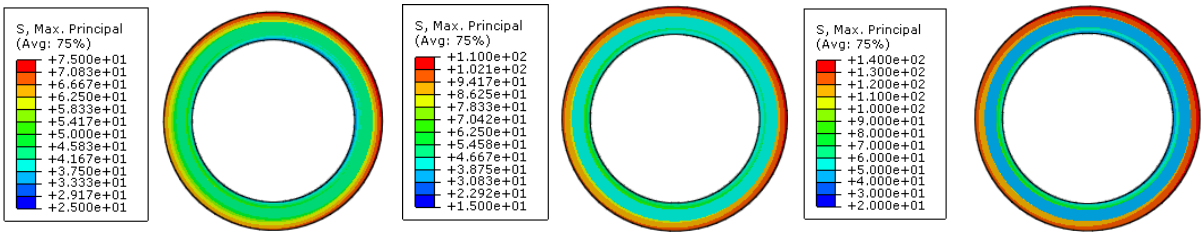

(a) 70 mmHg (b) 120 mmHg (c) 150 mmHg

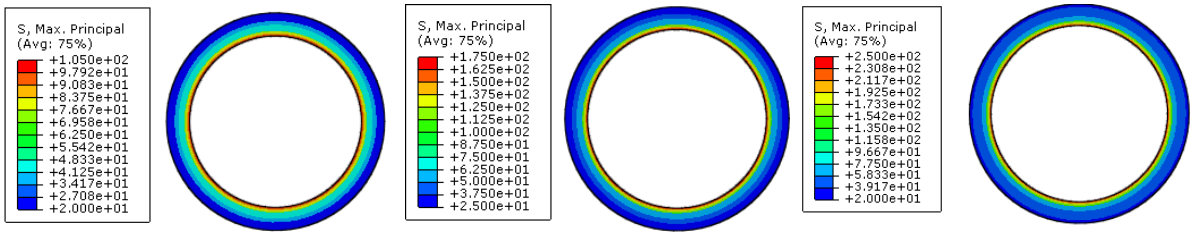

(d) 70 mmHg (e) 120 mmHg (f) 150 mmHg

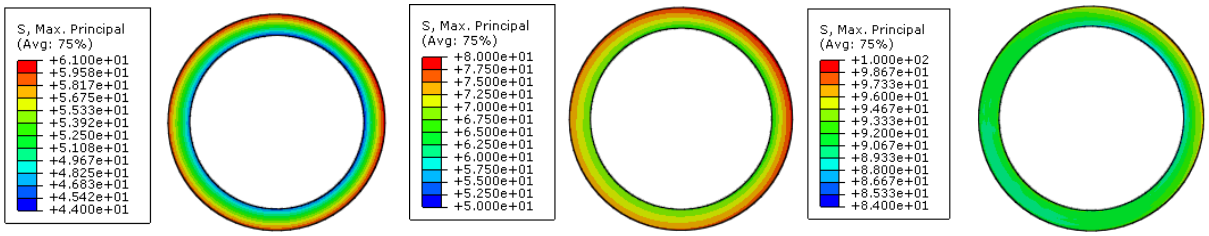

(g) 70 mmHg (h) 120 mmHg (i) 150 mmHg

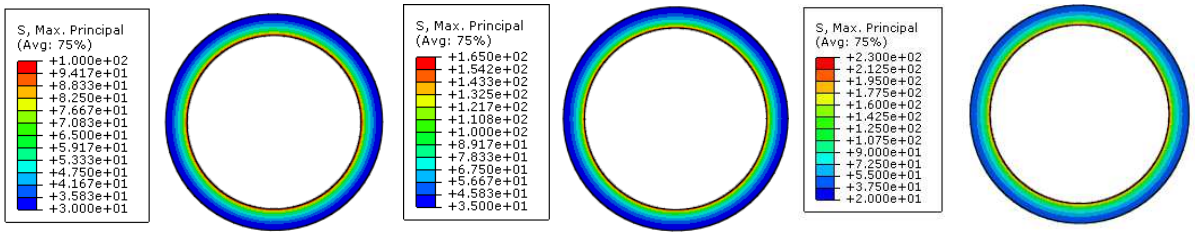

(j) 70 mmHg (k) 120 mmHg (ℓ) 150 mmHg

Fig. 11. Circumferential stress under diastolic (70 mmHg), physiological systolic (120 mmHg) and supra-physiological systolic (150 mmHg) internal pressure and residual stress (kPa). First row: three-layer model with residual stresses; second row: three- layer model without residual stresses; third row: one- layer model with residual stresses; and fourth row: one- layer model without residual stresses.

and insignificant for the radial stress distribution. It is important to note that for supra-physiological systolic pressure in the monolayer model, the circumferential and longitudinal stresses are uniform along the thickness of the wall aorta.

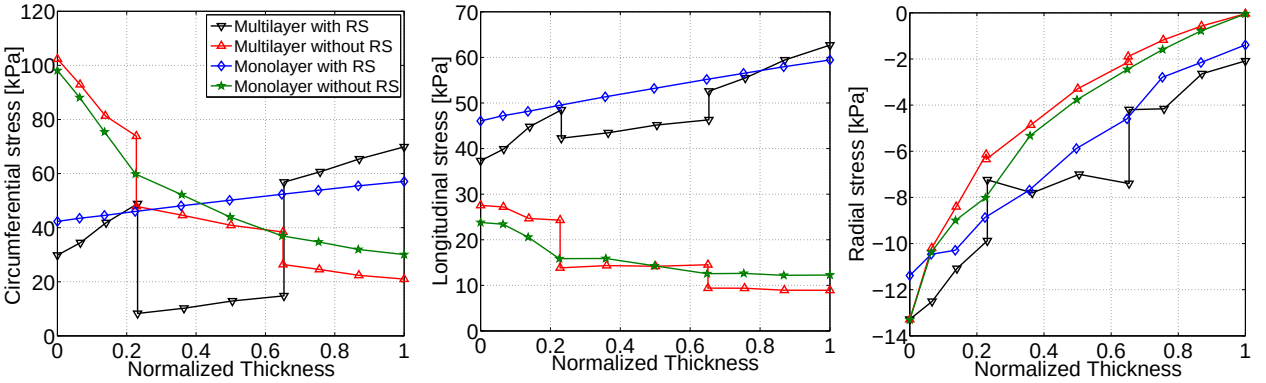

(a) Circ stress 70 mmHg (b) Long stress 70 mmHg (c) Rad stress 70 mmHg

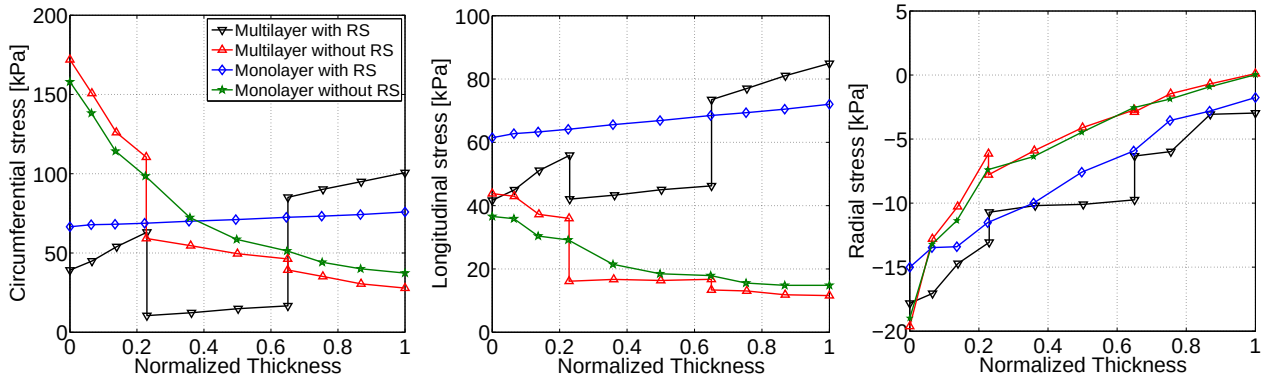

(d) Circ stress 120 mmHg (e) Long stress 120 mmHg (f) Rad stress 120 mmHg

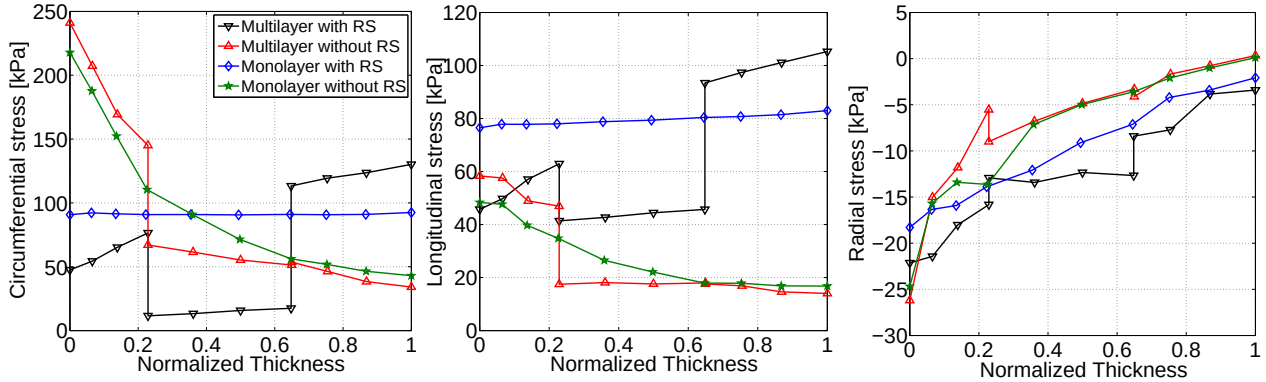

(g) Circ stress 150 mmHg (h) Long stress 150 mmHg (i) Rad stress 150 mmHg

Fig. 12. Circumferential, longitudinal and radial stress variation (kPa) across the normalized thickness [-] under diastolic (70 mmHg), physiological systolic (120 mmHg) and supra-physiological systolic (150 mmHg) internal pressures for the three- layer model with and without residual stresses and the one- layer model with and without residual stresses. Note that discontinuity of the radial stress distributions at the interfaces between layers and no vanish value at the outer radius are due to stress are computed on the integration points instead of the nodes.

4 Discussion

Most of the existing computational models developed for the simulation of cardiovascular devices have modeled the non-diseased arterial wall as a homogeneous and single-layer structure (García et al., 2012; Gasser and Holzapfel, 2007; Migliavacca et al., 2005) and more recently as a three-layer structure without residual stresses (Conway et al., 2014; Holzapfel et al., 2005b, 2002; Sáez et al., 2012; Zahedmanesh et al., 2010). It is considered in the literature that the three-layer model approximates the mechanics of the arterial wall better than the single-layer model. However, to the best of the authors' knowledge, this hypothesis has not been verified to date.

Our hypothesis was that the multilayer model can only reproduce the response of the whole aorta if the layer- specific residual stresses are included. To test this hypothesis, we compared the experimental results of uniaxial and biaxial tests of the whole aorta with the numerical results obtained by FE simulations of a multilayer model where the experimental residual stresses and mechanical properties of each separated layer were considered. Our results demonstrate that substantial differences between the multilayer models and the experimental results can be observed when residual stresses are neglected. Both phenomenological and microstructural multilayer models reproduce the response of the whole aorta when residual stresses are included in a similar way, with small differences in uniaxial cases. However, when the material parameters obtained using uniaxial tests are considered to capture the biaxial response, the GOH model using microstructural parameters reproduces better results than the same model using phenomenological parameters, show- ing the better capability of the microstructural properties to reproduce different stress states in spite of the worse fitting in the uniaxial tests. Due to the solution is not unique, the fitted parameters should be no physical meaning. It is possible that two totally different solutions give the same value of the cost function but when implemented in the whole-layer FE model each solution provide a different response when the parameters κ and θ are considered as phenomenological parameters. For this reason, it is better working a model when the structural parameters κ and θ are derived from experiments.

The results also demonstrate that there is a discontinuity stress map caused by the inhomogeneous composition of the multilayer model. The combined effect of prestress and the load exerted by the clamps reduces the stress discontinuity showing a quasi-uniform stress distribution along the sample thickness. This is consistent with the well-known hypothesis that the main effect of residual stresses is to decrease the transmural gradient of stresses (Chaudhry et al., 1997; Chuong and Fung, 1986; Peterson and Okamoto, 2000).

After validation of the multilayer model, we built an idealized cylindrical aorta model to analyze the effect of the multilayer model vs the monolayer model with and without residual stresses on the mechanical response of the whole aorta. The results obtained show that including the three-layer model with residual stresses reduces the stress gradient for the three considered pressures, especially for the diastole and systole pressures in the physiological range (70 and 120 mmHg). However, for the single-layer model with residual stresses, the uniform stress distribution is given for systole pressures (120 and 150 mmHg). In contrast, using a three-

layer model without residual stresses provides similar results as a monolayer model, without relevant differences between the two models. These results contradict the view established in the literature that a three-layer model without residual stresses provides better results than a single-layer model. The stress distribution provided by the three-layer models without residual stress is similar to the single-layer model, showing a distribution with the maximum stress value on the inner radii of the aorta and the minimum stress value on the outer, see Figure 12.

Although the most realistic results are obtained using the multilayer model with residual stresses, it is very complicated to obtain the residual stresses for the intima, media and adventitia layers, especially in vessels with a smaller diameter than that of the aorta. To the best of the authors' knowledge, the studies by Sommer et al. (2010) on human carotid arteries, Peña et al. (2015) on porcine aortas, Sokolis et al. (2012); Sassani et al. (2015b,a) on ascending thoracic aortic aneurysms and Amabili et al. (2019) on human aorta are the only works that present the layer-specific mechanical properties and residual stresses at the same time.

The results presented herein could explain the unphysiological stress values in the intima obtained in some works that consider a coronary multilayer model using the mechanical properties of the intima, media and adventitia obtained by Holzapfel et al. (2005a). For example in Cilla et al. (2012), the maximum stress value on healthy intima without residual stress was around 800 kPa for physiological pressure. This value was reduced when a constant opening angle was considered for the whole aorta, demonstrating that the mechanical properties should be considered only if residual stresses are included.

Several limitations of the model presented in this paper should be noted. All the FE computations were conducted under the assumption of homogeneity, which clearly is not the case for arteries. Another limitation is that we used an average thickness in the FE analysis. Furthermore, using a specific 3D FE model reflecting the thickness variability along the sample would lead to a more accurate calculation of the stress values. However, the good agreement between the experimental and computational values obtained for the uniaxial and biaxial tests appear to show that these factors are not relevant to the outcome. The presented analysis treats the intima as load-bearing and thick structure which would only make sense if some part of the the media (internal elastic lamina) would be attached to the intima during layer separation or in human aortas in which intimal hyperplasia and/or atherosclerotic disease have greatly thickened the layer. Note that intima thickness of the sample II from Peña et al. (2015) was the thicker sample, the mean ratio between total wall thickness to inner diameter on that paper was 0.025 close to the ratio mentioned by other authors (Sokolis, 2015; Amabili et al., 2019). This limitation would be considered when analyzing the transmural stress distributions. The opening of circumferential rings was considered in the kinematic analysis while the curling of axial strips was disregarded. So the axial residual stretches which represent the curling of strips when cut from the intact aorta and the further curling and stretching when the entire wall axial strip is separated to its layers have been disregarded. We consider only the axial layer-specific stretches defined as the entire wall length divided by the layer length but no axial opening angles were considered (Holzapfel and Ogden, 2009). Because of the axial stresses due to λ_z^{res} are high and the good results fitting the whole experiments using the partial axial pre-stretch, we hypothesized that they are negligible. To compare the experimental results of

uniaxial experiments with the numerical one obtained by FE simulations, we analyze only the force-displacement curves in the load direction and ignore the lateral response. The lateral displacements of the specimens during the uniaxial test should be measured and compared with the predictions using FE models. However, differences in the lateral response probably would be related to the incompressibility and material model more than the residual stresses. Finally, it is unclear to what extent the material properties of postmortem tissue samples differ from their *in vivo* properties.

In spite of these limitations, some contributions have been presented in this paper. First, we demonstrate that an appropriate multilayer model should include the layer- specific residual stresses. Second, a multilayer model without residual stresses presents the similar stress distribution as a monolayer model without residual stresses. Third, if layer-specific residual stresses are not available, there is less error on the stress distribution using a monolayer model with residual stresses than a multilayer model without residual stresses. The final aim of arterial numerical simulations is to help clinicians to appropriately diagnose and treat arterial pathologies. The contributions referred to above may be inappropriate for generalization, since they are based on the computation of only one investigated aorta sample. However, the aim of this paper is to discuss and verify the capability of the multilayer model to capture the whole response of the aorta obtained by experimental data and its influence on the stress distribution along the wall. It was not intended to study a larger number of aorta samples and to draw general conclusions on a statistical basis. In summary, existing multilayer models do not consider residual stresses showing results which are far from the physiological domain.

Acknowledgements

The authors gratefully acknowledge research support from the Spanish Ministry of Science and Technology through research projects DPI2016-76630-C2-1-R and PID2019-107517RB-I00, the regional Government of Aragón support for the funding of the research project LMP121-18 and T24-20R, the University of Zaragoza for the use of the Servicio General de Apoyo a la Investigación-SAI. CIBER Actions are financed by the Instituto de Salud Carlos III with assistance from the European Regional Development Fund. Part of the work was performed by the ICTS "NANBIOSIS" specifically by the Tissue & Scaffold Characterization Unit (U13) and High Performance Computing Unit (U27), of the CIBER in Bioengineering, Biomaterials & Nanomedicine (CIBER-BBN at the University of Zaragoza).

References

Alastrué, V., Peña, E., Martínez, M. A., Doblaré, M., 2007. Assessing the use of the "opening angle method" to enforce residual stresses in patient-specific arteries. Ann Biomed Eng 35, 1821–1837.

Amabili, M., Balasubramanian, P., Bozzo, I., Breslavsky, I. D., Ferraria, G., 2019. Layer-specific

hyperelastic and viscoelastic characterization of human descending thoracic aortas. J Mech Behav Biomed 99, 27–46.

Badel, P., Avril, S., Lessner, S., Sutton, M., 2012. Mechanical identification of layer-speciffic properties of mouse carotid arteries using 3D-DIC and a hyperelastic anisotropic constitutive model. Comput Methods Biomech Biomed Engin 15, 37–48.

Bellin, C., Ferruzzi, J., Roccabianca, S., Martino, E. S. D., Humphrey, J. D., 2013. A microstructurally motivated model of arterial wall mechanics with mechanobiological implications. Ann Biomed Eng 42, 488–50.

Calvo, B., Peña, E., Martínez, M. A., Doblaré, M., 2007. An uncoupled directional damage model for fibered biological soft tissues. Formulation and computational aspects. Int J Numer Meth Engng 69, 2036–2057.

Canham, P. B., Finlay, H. M., Boughner, D. R., 1997. Contrasting structure of the saphenous vein and internal mammary artery used as coronary bypass vessels. Cardiovasc Res 34, 557–567.

Canham, P. B., Finlay, H. M., Dixon, J. G., Boughner, D. R., Chen, A., 1989. Measurements from light and polarised light microscopy of human coronary arteries fixed at distending pressure. Cardiovasc Res 23, 973–982.

Carew, T. E., Vaishnav, R. N., Patel, D. J., 1968. Compressibility of the arterial wall. Circ Res 23, 61–86.

Chaudhry, H. R., Bukiet, B., Davis, A., Ritter, A. B., Findley, T., 1997. Residual stress in oscillating thoracic arteries reduce circumferential stresses and stress gradient. J Biomech 30, 57–62.

Chuong, C. J., Fung, Y. C., 1986. On residual stress in arteries. ASME J Biomech Eng 108, 189–192.

Cilla, M., Peña, E., Martínez, M. A., 2012. 3d computational parametric analysis of eccentric atheroma plaque: influence of axial and circumferential residual stresses. Biomechan Model Mechanobiol 11, 1001–1013.

Conway, C., McGarry, J., McHugh, P., 2014. Modelling of atherosclerotic plaque for use in a computational test-bed for stent angioplasty. Ann of Biomed Eng 42, 2425–2439.

Demiray, H., 1972. A note on the elasticity of soft biological tissues. J Biomech 5, 309–311.

Deveja, R. P., Iliopoulos, D. C., Kritharis, E. P., Angouras, D. C., Sfyris, D., Papadodima, S. A., Sokolis, D. P., 2018. Effect of Aneurysm and Bicuspid Aortic Valve on Layer-Specific Ascending Aorta Mechanics. Ann Thorac Surg 106, 1692–701.

Fung, Y. C., 1993. Biomechanics. Mechanical properties of living tissues, 2nd Edition. Springer-Verlag, New York.

García, A., Peña, E., Laborda, A., Lostalé, F., de Gregorio, M. A., Doblaré, M., Martínez, M. A., 2011. Experimental study and constitutive modelling of the passive mechanical properties of the porcine carotid artery and its relation to histological analysis. Implications in animal cardiovascular device trials. Med Eng Phys 33, 665–676.

García, A., Peña, E., Martínez, M. A., 2012. Influence of geometrical parameters on radial force during self-expanding stent deployment. Application for a variable radial stiffness stent. J Mech Behav Biomed 10, 166–175.

Gasser, T. C., Gallinetti, S., Xing, X., Forsell, C., Swedenborg, J., Roy, J., 2012. Spatial orientation of collagen fibers in the abdominal aortic aneurysm's wall and its relation to wall mechanics. Acta Biomat 8, 3091–3103.

Gasser, T. C., Holzapfel, G. A., 2007. Finite element modeling of balloon angioplasty by considering overstretch of remnant non-diseased tissues in lesions. Comput Mech 40, 47–60.

Gasser, T. C., Ogden, R. W., Holzapfel, G. A., 2006. Hyperelastic modelling of arterial layers with distributed collagen fibre orientations. J R Soc Interface 3, 15–35.

Gundiah, N., Ratcliffe, M. B., Pruitt, L. A., 2009. The biomechanics of arterial elastin. J Mech Behav Biomed Mater 2, 288–296.

Heo, S., Xu, Y., 2001. em[Heo and Xu(2001)] , 2001. constructing fully symmetric cubature formulae for the sphere. Math Comput 70, 269–279.

Holzapfel, G. A., Gasser, C. T., Sommer, G., Regitnig, P., 2005a. Determination of the layer-specific mechanical properties of human coronary arteries with non-atherosclerotic intimal thickening, and related constitutive modelling. Am J Physiol Heart Circ Physiol 289, H2048–H2058.

Holzapfel, G. A., Gasser, T. C., Ogden, R. W., 2000. A new constitutive framework for arterial wall mechanics and a comparative study of material models. J Elasticity 61, 1–48.

Holzapfel, G. A., Gasser, T. C., Ogden, R. W., 2004. Comparison of a multi-layer structural model for arterial walls with a fung-type model, and issues of material stability. ASME J Biomech Eng 126, 264–275.

Holzapfel, G. A., Ogden, R. W., 2009. Constitutive modelling of passive myocardium: a structurally based framework for material characterization. Phil Trans R Soc A 367, 3445–3475.

Holzapfel, G. A., Ogden, R. W., 2010. Modelling the layer-specific 3d residual stresses in arteries, with an application to the human aorta. J R Soc Interface 7, 787–799.

Holzapfel, G. A., Sommer, G., Auer, M., Regitnig, P., Ogden, R. W., 2007. Layer-specific 3d residual deformations of human aortas with non-atherosclerotic intimal thickening. Ann Biomed Eng 35, 530–545.

Holzapfel, G. A., Stadler, M., Gasser, T. C., 2005b. Changes in the mechanical environment of stenotic arteries during interaction with stents: computational assessment of parametric stent designs. ASME J Biomech Eng 127, 166–180.

Holzapfel, G. A., Stadler, M., Schulze-Bauer, C. A. J., 2002. A layer specific three-dimensional model for the simulation of balloon angioplasty using magnetic resonance imaging and mechanical testing. Ann Biomed Eng 30, 753–767.

Humphrey, J. D., 2002. Continuum biomechanics of soft biological tissues. Proc R Soc Lond A 175, 1–44.

Lillie, M. A., Shadwick, R. E., Gosline, J. M., 2010. Mechanical anisotropy of inflated elastic tissue from the pig aorta. J Biomech 43, 2070–2078.

Lu, X., Yang, J., Zhao, J. B., Gregersen, H., Kassab, G. S., 2003. Shear modulus of porcine coronary artery: contributions of media and adventitia. Am J Physiol Heart Circ Physiol 285, H1966–H1975.

Maes, L., Fehervary, H., Vastmans, J., Mousavi, J., Avril, S., Famaey, N., 2019. Constrained mixture modeling affects material parameter identification from planar biaxial tests. J Mech Behav Biomed 95, 124–135.

Migliavacca, F., Petrini, L., Montanari, V., Quagliana, I., Auricchio, F., Dubini., G., 2005. A predictive study of the mechanical behaviour of coronary stents by computer modelling. Med Eng Phys 27, 13–18.

Mousavi, J., Avril, S., 2017. Patient-specific stress analyses in the ascending thoracic aorta using a finite-element implementation of the constrained mixture theory. Biomechan Model

Mechanobiol 16, 1765–1777.
Nelder, J. A., Mead, R., 1965. A simplex method for function minimization. Computer J 7, 308–313.
Pandit, A., Lu, X., Wang, C., Kassab, G. S., 2005. Biaxial elastic material properties of porcine coronary media and adventitia. Am J Physiol Heart Circ Physiol 288, H2581–H2587.
Peña, J. A., Corral, V., Martínez, M. A., Peña, E., 2018. Over length quantification of the multiaxial mechanical properties of the ascending, descending and abdominal aorta using Digital Image Correlation. J Mech Behav Biomed 77, 434–445.
Peña, J. A., Martínez, M. A., Peña, E., 2015. Layer-specific residual deformations and uniaxial and biaxial mechanical properties of thoracic porcine aorta. J Mech Behav Biomed 50, 55–69.
Peterson, S. J., Okamoto, R. J., 2000. Effect of residual stress and heterogeneity on circunferencial stress in the arterial wall. ASME J Biomech Eng 122, 454–456.
Rhodin, J. A. G., 1980. Architecture of the vessel wall, Handbook of Physiology, The Cardiovascular System, vol. 2. American Physiological Society, Bethesda, MD.
Sassani, S. G., Kakisis, J., Tsangaris, S., Sokolis, D. P., 2015a. Layer-dependent wall properties of abdominal aortic aneurysms: Experimental study and material characterization. J Mech Behav Biomed 49, 141–161.
Sassani, S. G., Tsangaris, S., Sokolis, D. P., 2015b. Layer- and region-specific material characterization of ascending thoracic aortic aneurysms by microstructure-based models. J Biomech 48, 3757–3765.
Sáez, P., Alastrué, V., Peña, E., Doblaré, M., Martínez, M. A., 2012. Anisotropic microsphere-based approach to damage in soft fibered tissue. Biomechan Model Mechanobiol 11, 595–608.
Sáez, P., García, A., Peña, E., Gasser, T. C., Martínez, M. A., 2016. Microstructural quantification of collagen fiber orientations and its integration in constitutive modeling of the porcine carotid artery. Acta Biomat 33, 183–193.
Smith, J. F., Canham, P. B., Starkey, J., 1981. Orientation of collagen in the tunica adventitia of the human cerebral artery measured with polarized light and the universal stage. J Ultrastruct Res 77, 133–45.
Sokolis, D. P., 2015. Effects of aneurysm on the directional, regional, and layer distribution of residual strains in ascending thoracic aorta. J Mech Behav Biomed 46, 229–243.
Sokolis, D. P., 2019. Regional distribution of layer-specific circumferential residual deformations and opening angles in the porcine aorta. J Biomech 96, 106335 1–9.
Sokolis, D. P., Kritharis, E. P., Iliopoulos, D. C., 2012. Effect of layer heterogeneity on the biomechanical properties of ascending thoracic aortic aneurysms. Med Biol Eng Comput 50, 1227–1237.
Sommer, G., Regitnig, P., Költringer, L., , Holzapfel, G. A., 2010. Biaxial mechanical properties of intact and layer-dissected human carotid arteries at physiological and supra-physiological loadings. Am J Physiol Heart Circ Physiol 298, H898–912.
Spencer, A. J. M., 1971. Theory of Invariants. In: Continuum Physics. Academic Press, New York, pp. 239–253.
Wan, W., Hansen, L., Jr., R. L. G., 2010. A 3-D constrained mixture model for mechanically mediated vascular growth and remodeling. Biomech Model Mechanobiol 9, 403–419.
Weisbecker, H., Pierce, D. M., Regitnig, P., Holzapfel, G. A., 2012. Layer-specific damage experiments and modeling of human thoracic and abdominal aortas with non-atherosclerotic intimal thickening. J Mech Behav Biomed 12, 93–106.

Zahedmanesh, H., Kelly, D. J., Lally, C., 2010. Simulation of a balloon expandable stent in a realistic coronary artery: Determination of the optimum modelling strategy. Journal of Biomechanics 43 (11), 2126–2132.